Cell. Mol. Life Sci. (2010) 67:2979–2989
DOI 10.1007/s00018-010-0368-9

Cellular and Molecular Life Sciences

RESEARCH ARTICLE

Superactive mutants of thromboxane prostanoid receptor: functional and computational analysis of an active form alternative to constitutively active mutants

Manuela Ambrosio · Francesca Fanelli · Silvia Brocchetti · Francesco Raimondi · Mario Mauri · G. Enrico Rovati · Valérie Capra

Received: 2 November 2009 / Revised: 22 March 2010 / Accepted: 25 March 2010 / Published online: 11 April 2010

Abstract In class A GPCRs the E/DRY motif is critical for receptor activation and function. According to experimental and computational data, R3.50 forms a double salt bridge with the adjacent E/D3.49 and E/D6.30 in helix 6, constraining the receptor in an inactive state. The disruption of this network of interactions facilitates conformational transitions that generate a signal or constitutive activity. Here we demonstrate that non-conservative substitution of either E129$^{(3.49)}$ or E240$^{(6.30)}$ of thromboxane prostanoid receptor (TP) resulted in mutants characterized by agonist-induced more efficient signaling properties, regardless of the G protein coupling. Results of computational modeling suggested a more effective interaction between G_q and the agonist-bound forms of the TP mutants, compared to the wild type. Yet, none of the mutants examined revealed any increase in basal activity, precluding their classification as constitutively active mutants. Here, we propose that these alternative active conformations might be identified as superactive mutants or SAM.

M. Ambrosio · S. Brocchetti · G. E. Rovati (✉) · V. Capra
Laboratory of Molecular Pharmacology,
Department of Pharmacological Sciences,
Università degli Studi di Milano, Via Balzaretti 9,
20133 Milan, Italy
e-mail: genrico.rovati@unimi.it

F. Fanelli · F. Raimondi
Department of Chemistry and Dulbecco Telethon Institute,
Università di Modena e Reggio Emilia, Modena, Italy

M. Mauri
Department of Experimental Medicine,
Università di Milano-Bicocca, Monza, Italy

Keywords G protein-coupled receptor · E/DRY motif · Constitutive activity · Thromboxane receptor · Computational modeling

Introduction

G protein-coupled receptors (GPCRs) regulate virtually all known physiological processes in mammals [1], and the high proportion of drugs that target these receptors as agonists or antagonists recognize their significance to the current clinical practice of medicine [2]. This study focuses on the thromboxane prostanoid receptor (TP), a GPCR of the rhodopsin family that mediates the actions of thromboxane A2 (TXA_2), a product of arachidonic acid metabolism, and of isoprostanes, bioactive lipids that are produced in response to oxidative stress. TXA_2 is a potent inducer of platelet aggregation, vasoconstriction, mitogenesis, and angiogenesis, and plays important roles in inflammation, atherothrombosis, and cancer [3]. Human TP exists as two alternatively splice variants, TPα and TPβ, with different C-terminal cytoplasmic tails, which are usually co-expressed in cells [4] and can form homo- and hetero-oligomers [5].

Despite that many issues regarding GPCR function are still unclear, it is now accepted that in the rhodopsin-like family of GPCRs, several highly conserved motifs are critical in the process of receptor activation and function [6]. Particularly relevant seems to be the E/DRY motif at the end of helix 3 (H3) [7–9]. Consistent with in vitro and computational studies, in the inactive receptor states, R3.50 is engaged in a double salt bridge with the adjacent D/E3.49 and/or D/E6.30, while disruption of this network during receptor activation releases constraints on relative movement of the two helices [6, 7, 10]. Advances in

structure determination of rhodopsin provide high-resolution support to previous inferences, indicating that indeed in dark rhodopsin R3.50 is engaged in a double salt bridge with both E3.49 and E6.30 [11, 12], whereas the active opsin apoprotein shows a breakage of these bonds [13].

The two anionic partners of R3.50 are, however, expected not to be functionally equivalent. The significantly lower conservation of the E/D6.30 (i.e., 32%) compared to the E/D3.49 (i.e., 86%) [14] makes its potential role as a contributor of the inactive states valid only for a limited number of GPCRs [7], as demonstrated by the recent crystallographic structures of the inactive states of the β_1- and β_2-ARs and of the adenosine A_{2A} receptor ($A_{2A}R$). These structures do not hold the interhelical salt bridge, despite that all three crystals contain either a bond inverse agonist or antagonist and, thus, are likely to represent inactive states [15–18]. Assuming the lack of artifacts as recently argued [19], the crystal structures of these homologous GPCRs indeed suggest the existence of different inactive states, as it as been proposed by the ensemble theory [20, 21], which is based on the fact that receptors exist as collections of ensembles of numerous conformations.

In contrast, the highly conserved E/D3.49 is expected to be widely implicated in both stabilizing the inactive states and favoring the transitions towards the active ones through reprotonation of its side chain, as inferred from early in vitro and in silico experiments and from recent spectroscopic and structural studies on opsin [22–25, 26]. Accordingly, the irreversible neutralization by mutations of E/D3.49 was shown to increase basal activity, i.e., to induce constitutive activity (CA), and agonist-dependent activation in a variety of receptors, yet not in all [7, 8].

In a previous work investigating the ERY motif of TP we proposed that, unlike other GPCRs, $R130^{(3.50)}$ was involved in G protein coupling or recognition rather than in receptor activation [27]. It was, indeed, found that the increase in solvent accessibility near the E/DRY motif in response to agonist binding is instrumental in favoring the penetration of the C-term of $G\alpha_q$ in between the cytosolic ends of H3, H5, and H6 [28]. In line with these predictions, the recent crystallographic structures of the constitutively active opsin apoprotein show that the breakage of the salt bridge interactions between R3.50 and both E3.49 and E3.60, associated with about 200 $Å^2$ increases in solvent accessibility in the neighborhoods of the E/DRY motif compared to dark rhodopsin, favoring the establishment of interactions between the R3.50 itself and the peptide from transducin [13, 25].

In this study, the characterization of $E129^{(3.49)}$ and $E240^{(6.30)}$ mutants has been carried out to gather insights into the structural features of the inactive/active states of TP. In vitro experiments show that disruptive mutations at positions $E129^{(3.49)}$ (intrahelical bridge) or $E240^{(6.30)}$ (interhelical bridge) of TP generate receptors characterized by an agonist-induced increase in efficacy and/or potency in signaling, regardless of the G protein coupling without showing any increase in basal activity. As these active variants cannot be classified as CAM receptors as generally intended and the activation profile is consistent with variegated GPCR active state ensembles, we propose that they might be considered as alternative to CAM and identified as superactive mutants or SAM.

Materials and methods

cDNA for TP was kindly provided by Dr. Colin Funk (University of Pennsylvania, Philadelphia, PA). Cell-culture media, animal serum, supplements, Lipofectamine2000, Opti-MEM I, and molecular biology reagents were purchased from Invitrogen (Carlsbad, CA). The QuickChange Site-Directed Mutagenesis Kit and Epicurian Coli XL-1Blue competent cells were from Stratagene (La Jolla, CA). Inositol-free Dulbecco's modified Eagle's medium (DMEM) was from ICN Pharmaceuticals Inc. (Costa Mesa, CA). Ultima Gold was from PerkinElmer Life and Analytical Sciences (Boston, MA), as were [5,6-^{3}H]SQ29,548 and myo-[2-^{3}H]inositol. U46619, SQ29,548, and cAMP EIA Kit were from Cayman Chemical (Ann Arbor, MI). Anion exchange resin AG 1X-8 (formate form, 200–400 mesh) and Lowry dye-binding protein reagents were from Bio-Rad (Hercules, CA). Restriction and modification enzymes were purchased from Fermentas/M-Medical (Milan, Italy). Oligonucleotide synthesis and plasmid DNA sequencing were performed by MWG Biotech (Ebersberg, Germany). Plasmid DNAs were purified with QIAGEN (Hilden, Germany) specific kits. All other reagents of the highest purity were available from Sigma-Aldrich (St. Louis, MO).

Numbering of residues

Residues in TP receptor were given two numbering schemes. First, residues were numbered according to their positions in the human TPα receptor sequence. Second, residues were also indexed according to their position relative to the most conserved residue in the transmembrane domain in which it is located. By definition, the most conserved residue was assigned the position index "50" [29].

Construction of mutant TP receptors

Mutations at position $E129^{(3.49)}$ and $R130^{(3.50)}$ of TPα were previously obtained in our laboratory [27]. Specific $E240^{(6.30)}$ substitutions were introduced into the cDNA for

TPα using the QuikChange® Site-Directed Mutagenesis Kit according to the manufacturer's instructions. Briefly, the QuikChange site-directed mutagenesis method was performed using *PfuTurbo*® DNA polymerase and a thermal temperature cycler. The synthetic oligonucleotide primers containing the desired mutation ($E129^{(3.49)}N$, $E240^{(6.30)}V$, $E240^{(6.30)}K$, $E240^{(6.30)}Q$), each complementary to opposite strands of the plasmid vector, were extended during temperature cycling by *PfuTurbo* DNA polymerase. Incorporation of the oligonucleotide primers generated a mutated plasmid containing staggered nicks. Following temperature cycling, the product was treated with *Dpn*I to digest the parental DNA template and to select for mutation-containing synthesized DNA. The nicked vector DNA containing the desired mutations was then transformed into supercompetent cells (Epicurian Coli XL-1Blue). Mutant oligonucleotides were synthesized and sequenced and were as follows:

FW TP-E129N 5′-CCGCCATGGCCTCAAACCGGTA CCTGGGTATCAC-3′;
FW TP-E240V 5′-CCCAGCAGCGTCCCCGAGACTC CGTGGTGGAGATGATGGC-3′;
FW TP-E240K 5′-CCCAGCAGCGTCCTCGCGACTC CAAGGTGGAGATGATGGC-3′;
FW TP-E240Q 5′-CCCAGCAGCGTCCTCGCGACTC CCAGGTGGAGATGATGGC-3'.

Plasmid DNA was purified with the QIAprep Spin Miniprep Kit and sequenced. Ultrapure plasmids for cell transfections were obtained with the QIAfilter Plasmid Midi Kit.

Culture and transfection of COS-7 cells

COS-7 cells were cultured in DMEM supplemented with 10% fetal bovine serum (FBS), 2 mM glutamine, 50 U/ml penicillin, 100 μg/ml streptomycin, and 20 mM HEPES buffer, pH 7.4, at 37°C in a humidified atmosphere of 95% air and 5% CO_2. COS-7 cells were plated out into 12-well [total inositol phosphates (IPs) or cAMP assays] or 24-well (binding assay) tissue culture dishes previously coated with poly-D-lysine, following a standard seeding protocol to obtain a 50–60% confluence at the time of transfection. This was performed using Lipofectamine2000 according to the manufacturer's instructions. In brief, Lipofectamine2000/DNA transfection mix was prepared in Opti-MEM I Medium at an optimized 2:1 ratio. Cell medium was replaced before transfection with fresh DMEM supplemented with 10% FBS, and transfection mix was added to cells after 20-min incubation at room temperature to allow the complexes to form. Equal protein content was ensured at the end of each assay by the Lowry dye-binding procedure.

Ligand-binding assay

Receptor expression was monitored 48 h after transfection. A mixed-type protocol was performed as previously described [27, 30] on confluent adherent cells in 250 μl of serum-free DMEM containing 0.2% (w/v) BSA in the presence of 0.1–1 nM concentrations of the specific receptor antagonist [^{3}H]SQ29,548 (48 Ci/mmol) and 0.003–10 μM concentrations of the homologous or heterologous unlabeled ligand. After 30 min of incubation at 25°C, cells were washed with ice-cold PBS containing 0.2% (w/v) BSA and lysed in 0.5 N NaOH. Radioactivity was measured by liquid scintillation counting in Ultima Gold.

Total inositol phosphate quantitation

The functional activity of the receptor was assessed 48 h after transfection by quantification of the total labeled IPs using a conventional gravity flow column chromatography method as previously described [27]. In brief, the day before transfection, cells were labeled with 1 μCi of [*myo*-2-^{3}H]inositol (17 Ci/mmol) for 20 h in serum-free, inositol-free DMEM containing 20 mM HEPES buffer, pH 7.4, and 0.5% (w/v) Albumax I were incubated with 25 mM LiCl for 10 min. Following pretreatment with either SQ29,548 or vehicle, cells were stimulated with the agonist U46619, for 30 min. At the end of this period, the medium was removed and the cells were lysed by with 0.75 ml of 10 mM formic acid. Cell lysates were applied onto an anion exchange AG 1X-8 column, formate form, 200 to 400 mesh and the desired fraction eluted with 2 M ammonium formate/formic acid buffer at pH 5. Radioactivity was determined by liquid scintillation counting in Ultima Gold.

cAMP assay

Measurement of cAMP accumulation was performed 48 h after transfection using EIA Kit. All the solutions were in serum-free DMEM containing 0.5% (w/v) Albumax I and HEPES–NaOH 20 mM, pH 7.4. In brief, confluent cells at 37°C were preincubated with or without 100 μM BAPTA/AM for 60 min, pretreated with 500 μM IBMX for 10 min, and then stimulated with different concentrations of the agonist U46619 in the absence or presence of SQ29,548 for 10 min. Reaction was stopped by washing with ice-cold PBS and cell culture extracts were obtained by incubation with 0.1 M HCl for 20 min at 25°C, followed by centrifugation at 12,000 × *g* for 10 min at 4°C. Supernatants were assayed immediately after collection according to the manufacturer's instructions.

Computational modeling

In this study we have attempted an alternative way to model the active states of TP, i.e., by comparative modeling (by means of MODELLER) [31] by using the crystal structure of the constitutively active opsin apoprotein as a template (i.e., PDB code: 3CAP) [13]. All the receptor domains except for the C-term were modeled (i.e., 1–321 sequence). The sequence alignment employed in this study as well as the deletions in the opsin template are the same as the ones utilized in our previous computational modeling study [28]. α-Helix restraints were applied to the 47–54, 99–106, 268–273, and 283–294 amino acid stretches of the target receptors. These restraints resulted in one- or two-turn elongation of the intracellular ends of H1 and of the extracellular ends of H3, H6, and H7. The best TP model was subjected to rotations of the amino acid side chains when in non-allowed conformations and then subjected to energy minimization, following the docking of the U46619 agonist. The same minimization was applied to the agonist-bound forms of the E129$^{(3.49)}$V and E240$^{(6.30)}$V mutants. The minimized coordinates of the wild type (WT) and of the E129$^{(3.49)}$V and E240$^{(6.30)}$V mutants were subjected to rigid body docking simulations (by means of the ZDOCK program [32]) with heterotrimeric G_q. The latter was achieved by comparative modeling by using the $G\alpha_{i1}$ structure as a template (PDB code 1GP2 [33]). Different from the heterotrimeric G_q employed in the previous study [28], the G_q employed herein held the last ten amino acids in the same conformation as the recent X-ray structure of the transducin C-term (PDB code: 3DQB) [25]. The new model of the α-subunit was merged with the $\beta\gamma$-subunits extracted from the $G\alpha_{i1}\beta_1\gamma_2$ heterotrimer (i.e., PDB code: 1GP2) [33]. Docking simulations and analyses followed the protocol previously described [28]. Substantially similar reliable solutions were achieved for the three receptor forms due to the very low structural deviation between them [i.e., a Cα-atom root mean square deviation (Cα-RMSD) around 0.2 Å]. A systematic higher number of filtered solutions characterized the two mutants compared to the WT. Such solutions comprised a set similar to the selected complexes in our previous study [28] and another, characterized by about 90° rotation in the membrane plane around the main axis of α5, and by a more prominent penetration of the C-term of $G\alpha_q$ in the seven-helix bundle of TP. The latter docking mode, which approached that of the C-terminal peptide from transducin [25], was selected for molecular dynamics (MD) simulations. To start from TP–G_q complexes as much similar as possible, the best scored complex involving the WT (i.e., the solution ranked at the 89th position out of 4,000) was used to build the ones with E129$^{(3.49)}$V and E240$^{(6.30)}$V mutants. The complexes between GDP-bound G_q and the agonist-bound forms of WT and of the E129$^{(3.49)}$V and E240$^{(6.30)}$V mutants were energy minimized and then subjected to 15 ns MD simulations in implicit membrane/water. Whereas such simulation time is exceedingly short compared to the time scale of receptor or G protein activation, it is, however, adequate to infer differences in the helix, loops, and side-chain motions involving preformed complexes between Gq and the active-like structures of the three TP forms (i.e., WT as well as E129$^{(3.49)}$V and E240$^{(6.30)}$V mutants). Reduction of the system's degrees of freedom by using an implicit membrane/water model as well as the employment of intrahelix distance restraints helped in this respect. Intrahelix distance restraints were applied to the receptor as well as to all the α-helical segments in the $\alpha\beta\gamma$ subunits of G_q. A disulphide bridge was allowed to form between C105$^{(3.25)}$ and C183, in EL2. Energy minimizations and MD simulations were carried out by using the GBSW implicit membrane/water model [34]. Minimizations were carried out by using 1,500 steps of steepest descent followed by adopted basis Newton–Raphson (ABNR) minimization, until the root mean square gradient was <0.001 kcal/mol Å. With respect to the setup of MD simulations, the lengths of the bonds involving the hydrogen atoms were restrained by the SHAKE algorithm, allowing for an integration time step of 0.002 ps. The systems were heated to 300 K with 7.5 K rises every 2.5 ps per 100 ps by randomly assigning velocities from a Gaussian distribution. After heating, the system was allowed to equilibrate for 100 ps. The temperature of the systems was kept constant during the production phase.

Data and statistical analysis

All average results are presented as mean ± SD. When indicated, ANOVA followed by post hoc test for multiple comparisons was performed. Data from radioligand binding were evaluated by a nonlinear, least-squares curve-fitting procedure using GraphPad Prism version 4, implemented with the *n*-ligand *m*-binding site model, as described in the LIGAND computer program [35]. Monotonic concentration–response curves were evaluated using Prism 4, which use the four-parameters logistic model as described in the ALLFIT program [36]. Biphasic curves were analyzed in Prism 4 by implementing a modified version of the bell-shaped curve equation described in BELLFIT [37]:

$$\delta = \text{Bottom} + \frac{\text{Plateau}_1 - \text{Bottom}}{1 + 10^{(\text{Log EC}_{50\_1} - X)} \times b_1} + \frac{E_{\max} - \text{Plateau}_1}{1 + 10^{(\text{Log EC}_{50\_2} - X)} \times b_2}$$

where δ = response; X = Log concentration of the agonist; Bottom = response when $X = 0$; EC_{50_1} and

EC_{50_2} = concentrations of the agonist that produce half of the response of the first and second component, respectively; b_1 and b_2 = slopes of the first and second component, respectively; $Plateau_1$ = maximal response of the first component; E_{max} = response for an infinite concentration of X.

Parameter errors are all expressed in percentage coefficient of variation (%CV) and calculated by simultaneous analysis of at least three different independent experiments performed in duplicate or triplicate. Selection of the best fitting model has been performed using the statistical principle of the "extra sum of squares" [38]. A statistical level of significance of $p < 0.05$ was accepted. All curves shown are computer generated.

Results

Antagonist-binding analysis and receptor expression

Binding assays were performed with the specific antagonist [^{3}H]SQ29,548 in COS-7 cells transiently transfected with WT or mutant TP receptors, or pcDNA3 vector alone. Mock-transfected cells showed no binding to [^{3}H]SQ29,548 (data not shown). All receptors were expressed at a level sufficient to perform radioligand-binding analysis, yet, to allow a proper comparison of receptor response, conditions of transfection were adjusted to secure equivalent levels of receptor expression for WT and mutants as previously described [27]. Computer-assisted analysis of binding data from WT receptor and mutants revealed monophasic-binding curves fitting a single site model. Calculated affinity for the WT receptor was in the nanomolar range, as previously reported [27], and affinities for the mutant receptors were not statistically different from that of the WT (Table 1).

Table 1 Binding affinities of [^{3}H]SQ29,548 in COS-7 cells transiently expressing the WT or the mutant human TP receptors

Mutant	K_d (nM ± %CV)	B_{max} (pmol/mg prot ± %CV)	No. of experiments
WT	9.16 ± 19	0.53 ± 48	5
E129$^{(3.49)}$V	7.45 ± 15	0.29 ± 39	5
E129$^{(3.49)}$N	12.8 ± 23	0.71 ± 54	4
E240$^{(6.30)}$V	6.43 ± 16	0.78 ± 30	6
E240$^{(6.30)}$K	8.62 ± 17	0.42 ± 44	3
E240$^{(6.30)}$Q	9.38 ± 16	0.61 ± 25	3

Binding affinities and capacities were obtained by simultaneous analysis of several independent [^{3}H]SQ29,548 mixed-type experiments analyzed with GraphPad Prism version 4 implemented with the LIGAND model [35]

Agonist induced signaling of TP E129$^{(3.49)}$ and E240$^{(6.30)}$ mutants

We previously demonstrated in HEK293 cells that E129$^{(3.49)}$V mutant stimulated total IP formation with a significant tenfold lower EC_{50} and approximately a two-fold higher E_{max} than the WT receptor [27]. To further expand these observations, we investigated if this behavior was retained also on the secondary coupling of the TP to heterotrimeric G_s. To our experience, COS-7 cells are a more suitable cell system than HEK293 in cAMP assays. Therefore, we first validated COS-7 cells to behave as HEK293 cells in agonist-induced total IP formation and confirmed our previous findings [27] (Fig. 1a). Thus, E129$^{(3.49)}$V receptor was assessed for its ability to induce cAMP accumulation following stimulation with increasing concentrations of the stable TXA_2 analog U46619 (Fig. 1b, c). U46619 concentration–response curve of WT receptor was characterized by an EC_{50} value of 511 nM ± 33%CV, consistent with the literature [39]. Intriguingly, agonist stimulation of E129$^{(3.49)}$V generated a concentration–response curve that clearly extends for more than two orders of magnitude and was better resolved by a two-component model in computer-assisted analysis (Fig. 1b). Similar to what was obtained in total IP accumulation, E_{max} of E129$^{(3.49)}$V was almost three-fold higher than that of the WT receptor (163.4 ± 4 and 62.46 ± 4%CV, respectively—Fig. 1b). BAPTA/AM was then used to prevent cAMP generation following classical TP–G_q-mediated calcium release. Figure 1c shows that the concentration–response curve was still biphasic and, albeit the absolute response was reduced, EC_{50}s were not statistically different from those obtained in the absence of BAPTA/AM.

Receptors generated by insertion of conservative and non-conservative mutations in terms of charge and/or hydropathy at position E240$^{(6.30)}$V were then tested for total IP production following stimulation with 1 μM U46619 (Fig. 2a). The agonist-induced level of total IPs in COS-7 cells expressing E240$^{(6.30)}$Q and E240$^{(6.30)}$K was as high as in cells expressing WT, whereas a statistically significant ≈35% increase in IP production was observed in COS-7 cells expressing the non-conservative E240$^{(6.30)}$V ($p < 0.01$). E240$^{(6.30)}$V mutant was, thus, investigated in depth by performing agonist-induced concentration–response curves of both total IP and cAMP accumulation (Fig. 2b, c). Computer analysis of IP response showed that EC_{50} of E240$^{(6.30)}$V was approximately 20-fold leftward shifted with respect to that of the WT (4.07 nM ± 58%CV and 78.13 nM ± 57%CV, Fig 2b). The concentration–response curve for cAMP accumulation of E240$^{(6.30)}$V was also shifted to the left and clearly displayed a Hill slope less than unity ($p < 0.01$). Computer-assisted analysis indicated the two-components to have EC_{50} of 2.1 nM ± 95%CV

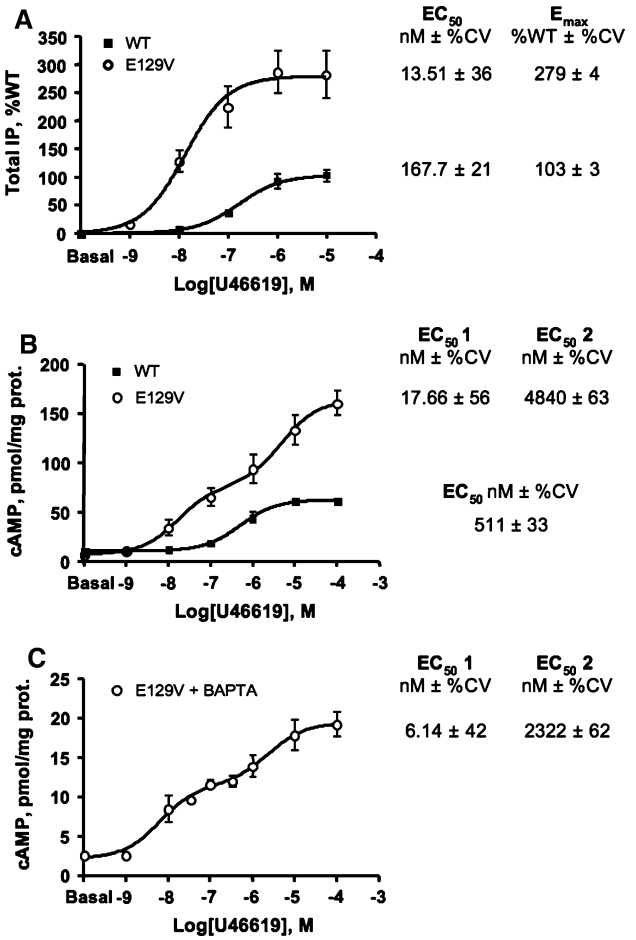

Fig. 1 Concentration–response curves of agonist-induced total IP and cAMP production in COS-7 cells expressing human TP WT or E129$^{(3.49)}$V mutant. **a** Total IPs were measured after incubation in the absence (basal) or presence of increasing concentrations of U46619 for 30 min. Data are expressed as percentage versus the maximal response induced by 10 μM agonist in the WT (1,110.7 dpm ± 120 SD, set as 100%). **b** cAMP was measured after stimulation in the absence (basal) or presence of increasing concentrations of U46619 for 10 min. **c** cAMP was measured after pretreatment with 100 μM BAPTA/AM for 60 min, followed by incubation in the absence (basal) or presence of increasing concentrations of U46619 for 10 min. Values of EC_{50} and E_{max} were obtained by simultaneous analysis with Prism (see "Materials and methods") of at least three independent experiments each performed in duplicates or triplicates. *Error bars* represent mean ± SE

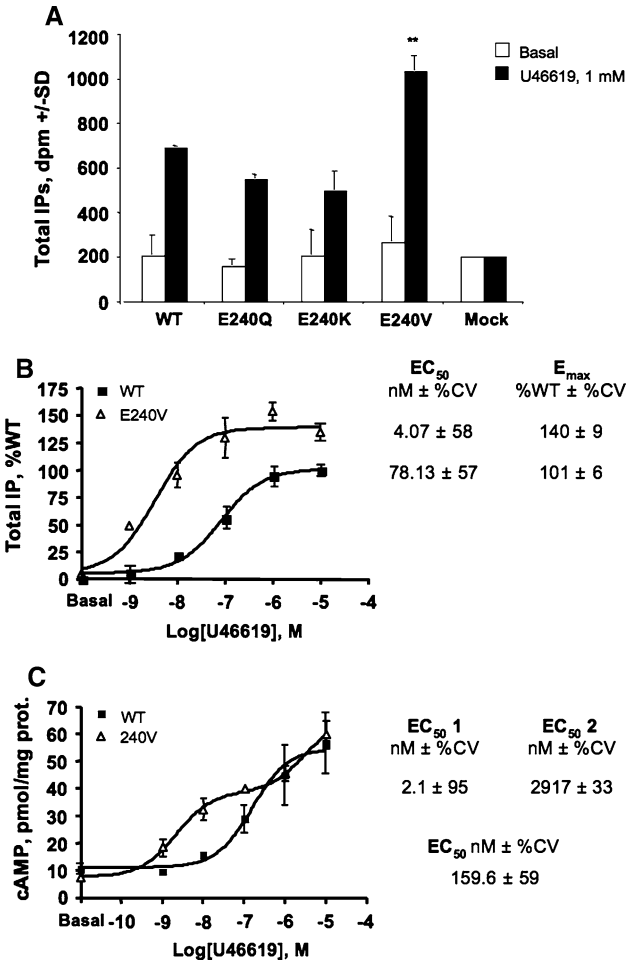

Fig. 2 Agonist-induced total IP and cAMP production in COS-7 cells expressing human TP WT or E240$^{(6.30)}$ mutants. **a** Total IPs were measured after incubation in the absence (basal) or presence of 1 μM U46619 for 30 min. Data are expressed as dpm ± SD, from at least three independent experiments each performed in triplicates (**$p < 0.01$ vs. WT; ANOVA followed by Bonferroni post hoc test). **b** Total IPs were measured after incubation in the absence (basal) or presence of increasing concentrations of U46619 for 30 min. Data are expressed as percentage versus the maximal response induced by 10 μM agonist in the WT (762 dpm ± 80 SD, set as 100%). **c** cAMP was measured after pretreatment with 100 μM BAPTA/AM for 60 min, followed by incubation in the absence (basal) or presence of increasing concentrations of U46619 for 10 min. Values of EC_{50} and E_{max} were obtained by simultaneous analysis with Prism (see "Materials and methods") of three independent experiments each performed in duplicates. *Error bars* represent mean ± SE

and 2,917 nM ± 33%CV, respectively, compared to 159.6 ± 59 for WT (Fig. 2c). E_{max} values resulted statistically different only for the IP response.

Analysis of basal activity and antagonist response

Basal activities of WT and mutated TP receptors were also assayed by analyzing their ability to activate production of total IPs or cAMP in the absence of agonist stimulation. None of the TP receptors exhibited CA, as mutant basal levels were not significantly different from those of the WT or the mock transfected cells (Fig. 3), all expressed at equal protein level. As a control, two known CAMs of the α_{1B}-AR, D142$^{(3.49)}$A and A293$^{(6.30)}$E [40, 41] were also tested. As expected, these CAMs displayed significant basal activity when expressed to a similar receptor level as the WT receptor ($p < 0.01$).

We also assessed the ability of the SQ29,549 to inhibit total IP production by WT, E129$^{(3.49)}$V, and E240$^{(6.30)}$V

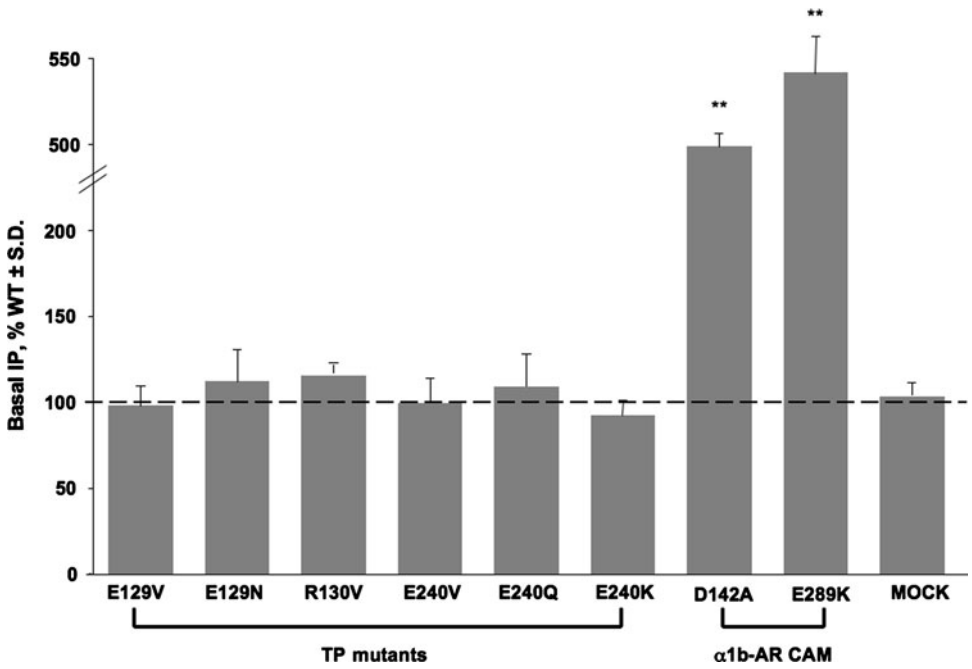

Fig. 3 Basal IPs content in COS-7 cells expressing WT, mutants of TP, and α1b-AR. Total IPs were measured in the absence of agonist stimulation. Transfection setting was adjusted to secure the equivalent level of receptor density for WT and mutants. Data are expressed as percentage versus WT, represented by the *horizontal dashed line* (405 dpm ± 48 SD for TP and 375 dpm ± 51 SD for α1b-AR, set as 100%), from at least two independent experiments each done in triplicates. $^{**}p < 0.01$ versus basal IPs of WT (ANOVA followed by Bonferroni post hoc test)

mutant receptors following stimulation with 1 μM U46619 (Fig. 4a). It is clear that the antagonist inhibition curves for E129$^{(3.49)}$V and E240$^{(6.30)}$V mutants showed a marked rightward shift ($p < 0.01$) with IC_{50} one order of magnitude higher than that of WT receptor ($IC_{50} = 0.14$ μM ± 38%CV for WT receptor vs. 2.4 μM ± 59%CV and 1.5 μM ± 60%CV for E129$^{(3.49)}$V and E240$^{(6.30)}$V, respectively). Similar results were obtained in cAMP assay (data not shown).

Agonist binding of TPα receptor mutants

WT and selected mutants transiently transfected in COS-7 cells were also tested for agonist binding to assess whether the mutations affected G protein coupling and/or activation. Heterologous competition curves of the unlabeled specific agonist U46619 versus [^{3}H]-SQ29,548 revealed a leftward shift for the E129$^{(3.49)}$V and E240$^{(6.30)}$V mutant curves compared to WT receptor curve (Fig. 4b), with a consequent increase in agonist affinity of about one order of magnitude ($K_i = 84$ nM ± 27%CV for WT receptor vs. 16 nM ± 26%CV and 7.8 nM ± 26%CV for E129$^{(3.49)}$V and E240$^{(6.30)}$V, respectively).

Discussion

Receptor pharmacology has been revolutionized by the discovery of inverse agonism [42, 43] and CA [40] providing insight into the mechanism of receptor activation [44–47]. The extended ternary complex model (TCM) introduced the view that the receptor has the intrinsic characteristic of existing in two discrete interconvertible conformations, one active state (R*), and one inactive state (R), which binds ligands with different affinities [44]. Several years of research indicate that the situation is more complex because GPCRs have a high degree of functional plasticity arising from structural flexibility and the ability of ligands to select and stabilize multiple conformations [48–50].

In a previous work we demonstrated that, unlike other GPCRs, non-conservative mutation at E129$^{(3.49)}$ of TP did not produce CA, but rather a receptor characterized by more efficient signaling properties, i.e., an increase in agonist affinity and potency as well as an increase in maximal efficacy for agonists compared to WT receptor [27]. This phenomenon has also been observed for other GPCRs, and has been interpreted as a mutation-specific conformational change toward an active-like conformation [8, 51]. Here we have utilized the TP receptor as a model to study the nature of intramolecular communication governing active and inactive forms of GPCRs. Our results demonstrate that non-conservative substitution of E129$^{(3.49)}$ within the ERY motif of TP results in a mutant characterized by agonist-induced higher efficacy and potency, not only with respect to $G_{q/11}$ coupling but also to G_s coupling.

As is the case for α_{1B}-AR and β_2-AR, TP also possess a E240$^{(6.30)}$, thus potentially being able to form interhelical bridges between H3 and H6. The non-conservative mutation E240$^{(6.30)}$V also produced a SAM with more efficient signaling properties, i.e., increase in agonist potency, for

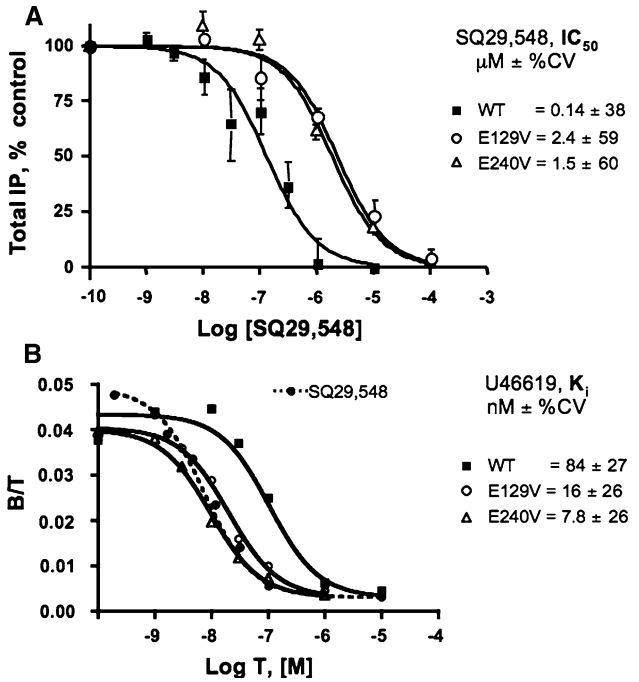

Fig. 4 Inhibition of SQ29,548 and competition of U46619 curves in TP WT and E129$^{(3.49)}$V or E240$^{(6.30)}$V mutants. **a** Analysis of SQ29,548 inhibition curves of 1 μM U46619-induced total IP production in COS-7 cells expressing human TP WT and E129$^{(3.49)}$V or E240$^{(6.30)}$V mutants. *Error bars* represent mean ± SE. **b** Agonist-binding studies in COS-7 transiently expressing WT and mutated TPα receptors. [^{3}H]SQ29,548 mixed type curves and U46619 heterologous competition curves are shown for WT, E129$^{(3.49)}$V and E240$^{(6.30)}$V mutant receptors. Binding is expressed as the ratio of bound ligand concentration to total ligand concentration (*B/T*, dimensionless) versus the logarithm of total unlabeled ligand concentration (Log *T*). Non-specific binding was calculated by computer as one of the unknown parameters of the model and was always <10% of total binding. Several independent heterologous competition experiments were performed, each in duplicate, and analyzed simultaneously. For the sake of clarity, only curves from one representative experiment for each receptor are shown

both $G_{q/11}$ and G_s signaling pathways and, efficacy, limited to IP production. Accordingly, the heterologous competition curves of the agonist U46619 versus [^{3}H]-SQ29,548 for both the E129$^{(3.49)}$V and E240$^{(6.30)}$ mutants revealed an increase in affinity of one order of magnitude versus WT receptor, a characteristic anticipated by the extended TCM [44], suggesting an increased coupling of the mutants with G proteins. Yet, reprotonation of E3.49 seems a fundamental requirement for receptor activation [7, 9], confirming that the two anionic partners of R3.50 are not functionally equivalent. These data, therefore, seem to suggest a major role for intrahelical bridges, than for interhelical ones in receptor activation.

Furthermore, particularly for the E129$^{(3.49)}$V mutant, cAMP concentration–response curves are biphasic, clearly spanning more that two orders of magnitude indicating a complex behavior of the U46619 agonist. Biphasic curves have also been obtained in the presence of BAPTA, excluding the existence of a cross talk between the cAMP and PC-PLC pathways using the intracellular machinery, leading to complex effects in whole cells. Computer-assisted analysis revealed the appearance of a high-potency component that is likely to reflect a peculiar receptor conformation. Despite that we do not have a clear molecular interpretation for this phenomenon, this high affinity/potency component might solely reflect a greater number of receptors in the active state or something more specific, such as a tendency to form a greater amount of dimers. In this regard, because TP forms both homo- and hetero-dimers, it might be interesting to bear in mind that a mutant TP receptor with a strong reduction in its tendency to form dimers showed a strong decrease in agonist potency compared to the WT receptor (unpublished observations). Taken together these data suggest that that the ability to form high-order structures might regulate the affinity/potency of TP for its agonist.

The hypothesis of induction of a particular receptor conformation is further supported by the shifting to the right of the SQ29,548 inhibition curve of the agonist-induced second messenger production in cells expressing E129$^{(3.49)}$V or E240$^{(6.30)}$V mutants compared to the WT receptor. Despite that all the mutants showed similar binding affinities to WT receptor for the labeled antagonist [^{3}H]SQ29,548, at least ten-fold increase in the antagonist concentration was necessary to inhibit E129$^{(3.49)}$V and E240$^{(6.30)}$V agonist-induced signaling.

In line with the hyper-stimulated activity shown by the two mutants, MD simulations of the three TP forms in complex with heterotrimeric G_q revealed a better propensity of R3.50 to perform a network of intra- and intermolecular connections at the receptor–G protein interface in the two mutants compared to WT. Such an effect is particularly marked in the E129$^{(3.49)}$V mutant, stressing the peculiar role of this conserved glutamate as a controller of the R3.50 motions through deprotonation/reprotonation of its side chain. In this respect, the establishment of the R130$^{(3.50)}$–N215$^{(5.57)}$ and R130$^{(3.50)}$–Q246$^{(6.36)}$ intramolecular as well as the R130$^{(3.50)}$–N344$^{Gq\alpha}$ intermolecular hydrogen bonds (H-bonds) in the mutant receptor forms is associated with a deeper receptor penetration by the C-term of $G_{q\alpha}$ and the consequent formation of a larger receptor–G protein interface than in the WT (Fig. 5). This can be appreciated by the larger solvent accessible surface (SAS) area in the cytosolic regions of the E129$^{(3.49)}$V mutant extracted from the complex with G_q, compared to the WT (Fig. 5). Collectively, these data suggest that the irreversible neutralization of either E129$^{(3.49)}$ or E240$^{(6.30)}$, with particular emphasis to the E/DRY glutamate, facilitate the formation and maintenance of the receptor-binding site for the G protein through

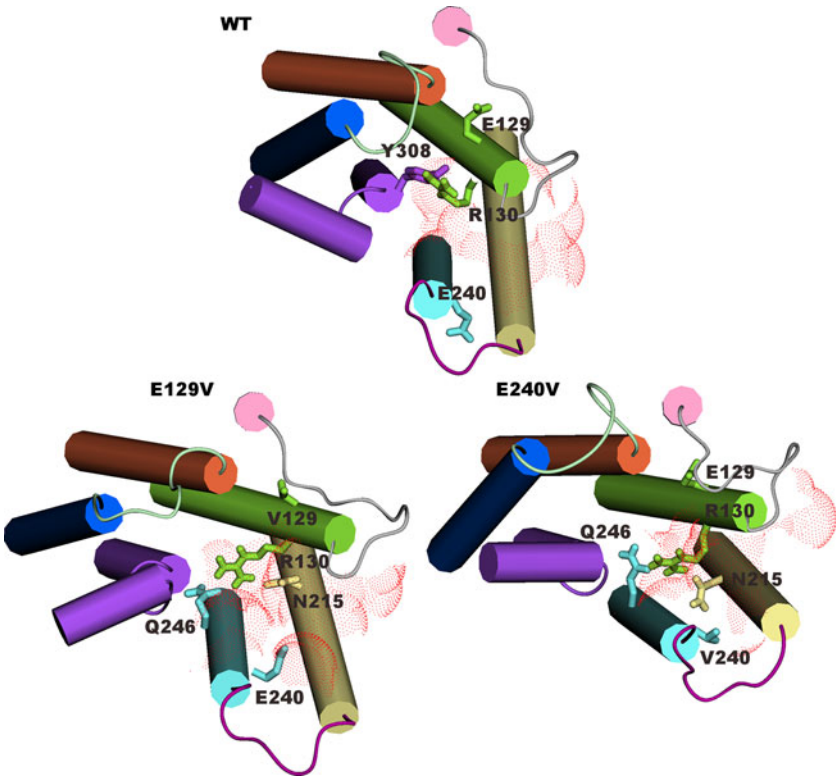

Fig. 5 Average minimized structures of WT and mutated agonist-bound TP. The structures have been extracted from the energy minimized receptor–G protein complexes averaged over the last 100 ps of 15 ns trajectories. Only the cytosolic and the seven-transmembrane domains are shown, seen from the intracellular side in a direction perpendicular to the membrane plane. Helices 1, 2, 3, 4, 5, 6, and 7 are colored in *blue*, *orange*, *green*, *pink*, *yellow*, *cyan* and *violet*, respectively, whereas EL1, EL2, and EL3 are colored in *light green*, *grey* and *purple*, respectively. Helix 8 is colored in *violet* as well. Details of the intramolecular interaction pattern of R3.50 of the E/DRY motif are shown, represented in *sticks*. The SAS computed over R130$^{(3.50)}$, I134$^{(3.54)}$, T135$^{(3.55)}$, N215$^{(5.57)}$, V219$^{(5.61)}$, L222$^{(5.63)}$, Y226$^{(5.67)}$, S239$^{(6.29)}$ and M243$^{(6.33)}$ is represented by *red dots*. The SAS for the WT, E129$^{(3.49)}$V and E240$^{(6.30)}$V is: 257.0, 369.0 and 282.0 Å^2, respectively

peculiar conformational changes of the highly conserved R130$^{(3.50)}$.

Yet, none of the TP mutants examined by our laboratory or other laboratories exhibited increased CA. We have previously demonstrated for the loss of function mutant R130V that the level of receptor expression does not alter basal activity [27], a feature governed by the R–R* equilibrium [52]. The same is also true for E129$^{(3.49)}$V and E240$^{(6.30)}$V mutants both for total IP and cAMP signaling components (data not shown). Thus, these findings clearly indicate that TP is refractory to CA, at least as far as the mutant considered. Furthermore, in our hands, the lack of effect of charge-neutralizing (e.g., E129$^{(3.49)}$N and E240$^{(6.30)}$Q) versus hydropathy-reversing mutants suggests that the conserved hydrophobic component of the network plays a central role in constraining the ground state of class A GPCRs.

On the basis of MD simulations of the TP in complex with heterotrimeric G_q we can speculate that the lack of CA in both the E129$^{(3.49)}$V and E240$^{(6.30)}$V mutants can be due to a strong coupling between agonist and G protein-binding domains of TP, whereby mutations near the G protein-binding sites require the presence of an agonist in the extracellular side to result in superefficient coupling. The existence of two-way intramolecular communication between the cytosolic domains and the ligand-binding site has been observed from previous [28] and present computational experiments.

In conclusion, pharmacological data complemented with computational experiments lead us to show that: (1) non-conservative substitution of E129$^{(3.49)}$ within the ERY motif of TP results in a mutant characterized by higher efficacy and potency, regardless of the G protein coupling; (2) non-conservative mutation of E240$^{(6.30)}$, proposed by computational modeling to interact with R130$^{(3.50)}$, also produces a mutant with more efficient signaling properties, i.e., increase in agonist potency, regardless of the G protein coupling; (3) the increase in agonist affinity/potency is confirmed by binding studies and by a ten-fold decrease in the antagonist potency in inhibit E129$^{(3.49)}$V and E240$^{(6.30)}$V agonist-induced total IP production; (4) cAMP concentration–response curves of E129$^{(3.49)}$V and

E240$^{(6.30)}$V showed a complex behavior spanning more than two orders of magnitude, likely to reflect a peculiar receptor conformation; (5) finally, the results of computational experiments suggest more effective interaction between G_q and the agonist-bound forms of the TP mutants, especially E129$^{(3.49)}$V, compared to the WT.

Therefore, here we propose to identify these mutant receptors as SAM, i.e., SAMs, to indicate possible alternative receptor conformations that can be shared by other GPCRs. SAMs, despite showing some of the characteristics of the active receptor states, lack the basic feature of a CAM receptor, i.e., the increase in basal activity.

Acknowledgments We acknowledge Dr. Tommaso Costa (Laboratory of Pharmacology, Istituto Superiore di Sanità, Roma, Italy) for exhaustive and useful discussions of the data and for critical assessment of the paper. We thank Dr. Susanna Cotecchia (Département de Pharmacologie et de Toxicologie, Lausanne, Switzerland) for providing CAM of the α_{1B}-AR. This work was supported in part by grants from EC FP6 (LSHM-CT-2004-005033 to GER). This study was also supported by a Telethon-Italy (S00068TELU to F.F.) and by a MIUR-FIRB grant (no. RBIN04CKYN to M.M.).

References

1. Lefkowitz RJ (2004) Historical review: a brief history and personal retrospective of seven-transmembrane receptors. Trends Pharmacol Sci 25:413–422
2. Tyndall JD, Sandilya R (2005) GPCR agonists and antagonists in the clinic. Med Chem 1:405–421
3. Nakahata N (2008) Thromboxane A2: physiology/pathophysiology, cellular signal transduction and pharmacology. Pharmacol Ther 118:18–35
4. Kinsella BT (2001) Thromboxane A2 signalling in humans: a 'Tail' of two receptors. Biochem Soc Trans 29:641–654
5. Laroche G, Lepine MC, Theriault C, Giguere P, Giguere V, Gallant MA, de Brum-Fernandes A, Parent JL (2005) Oligomerization of the alpha and beta isoforms of the thromboxane A2 receptor: relevance to receptor signaling and endocytosis. Cell Signal 17:1373–1383
6. Rosenbaum DM, Rasmussen SG, Kobilka BK (2009) The structure and function of G-protein-coupled receptors. Nature 459:356–363
7. Fanelli F, De Benedetti PG (2005) Computational modeling approaches to structure-function analysis of G protein-coupled receptors. Chem Rev 105:3297–3351
8. Rovati GE, Capra V, Neubig RR (2007) The highly conserved DRY motif of class A GPCRs: beyond the ground state. Mol Pharmacol 71:959–964
9. Vogel R, Mahalingam M, Ludeke S, Huber T, Siebert F, Sakmar TP (2008) Functional role of the "ionic lock"—an interhelical hydrogen-bond network in family A heptahelical receptors. J Mol Biol 380:648–655
10. Cotecchia S, Bjorklof K, Rossier O, Stanasila L, Greasley P, Fanelli F (2002) The alpha1b-adrenergic receptor subtype: molecular properties and physiological implications. J Recept Signal Transduct Res 22:1–16
11. Palczewski K, Kumasaka T, Hori T, Behnke CA, Motoshima H, Fox BA, Le Trong I, Teller DC, Okada T, Stenkamp RE, Yamamoto M, Miyano M (2000) Crystal structure of rhodopsin: a G protein-coupled receptor. Science 289:739–745
12. Teller DC, Okada T, Behnke CA, Palczewski K, Stenkamp RE (2001) Advances in determination of a high-resolution three-dimensional structure of rhodopsin, a model of G-protein-coupled receptors (GPCRs). Biochemistry 40:7761–7772
13. Park JH, Scheerer P, Hofmann KP, Choe HW, Ernst OP (2008) Crystal structure of the ligand-free G-protein-coupled receptor opsin. Nature 454:183–187
14. Mirzadegan T, Benko G, Filipek S, Palczewski K (2003) Sequence analyses of G-protein-coupled receptors: similarities to rhodopsin. Biochemistry 42:2759–2767
15. Rasmussen SG, Choi HJ, Rosenbaum DM, Kobilka TS, Thian FS, Edwards PC, Burghammer M, Ratnala VR, Sanishvili R, Fischetti RF, Schertler GF, Weis WI, Kobilka BK (2007) Crystal structure of the human beta2 adrenergic G-protein-coupled receptor. Nature 450:383–387
16. Cherezov V, Rosenbaum DM, Hanson MA, Rasmussen SG, Thian FS, Kobilka TS, Choi HJ, Kuhn P, Weis WI, Kobilka BK, Stevens RC (2007) High-resolution crystal structure of an engineered human beta2-adrenergic G protein-coupled receptor. Science 318:1258–1265
17. Warne T, Serrano-Vega MJ, Baker JG, Moukhametzianov R, Edwards PC, Henderson R, Leslie AG, Tate CG, Schertler GF (2008) Structure of a beta1-adrenergic G-protein-coupled receptor. Nature 454:486–491
18. Jaakola VP, Griffith MT, Hanson MA, Cherezov V, Chien EY, Lane JR, Ijzerman AP, Stevens RC (2008) The 2.6 angstrom crystal structure of a human A2A adenosine receptor bound to an antagonist. Science 322(5905):1211–1217
19. Mustafi D, Palczewski K (2008) Topology of class A G protein-coupled receptors: insights gained from crystal structures of rhodopsins, adrenergic and adenosine receptors. Mol Pharmacol 75(1):1–12
20. Onaran HO, Scheer A, Cotecchia S, Costa T (2000) A look into receptor efficacy. From the signalling network of the cell to the intramolecular motion of the receptor. In: Kenakin T, Angus J (eds) Handbook of experimental pharmacology. Springer, Berlin Heidelberg New York, pp 217–280
21. Kenakin T (2002) Efficacy at G-protein-coupled receptors. Nat Rev Drug Discov 1:103–110
22. Arnis S, Fahmy K, Hofmann KP, Sakmar TP (1994) A conserved carboxylic acid group mediates light-dependent proton uptake and signaling by rhodopsin. J Biol Chem 269:23879–23881
23. Scheer A, Fanelli F, Costa T, De Benedetti PG, Cotecchia S (1996) Constitutively active mutants of the alpha 1B-adrenergic receptor: role of highly conserved polar amino acids in receptor activation. EMBO J 15:3566–3578
24. Scheer A, Fanelli F, Costa T, De Benedetti PG, Cotecchia S (1997) The activation process of the alpha1B-adrenergic receptor: potential role of protonation and hydrophobicity of a highly conserved aspartate. Proc Natl Acad Sci USA 94:808–813
25. Scheerer P, Park JH, Hildebrand PW, Kim YJ, Krauss N, Choe HW, Hofmann KP, Ernst OP (2008) Crystal structure of opsin in its G-protein-interacting conformation. Nature 455:497–502
26. Madathil S, Fahmy K (2009) Lipid protein interactions couple protonation to conformation in a conserved cytosolic domain of G protein-coupled receptors. J Biol Chem 284:28801–28809
27. Capra V, Veltri A, Foglia C, Crimaldi L, Habib A, Parenti M, Rovati GE (2004) Mutational analysis of the highly conserved ERY motif of the thromboxane A2 receptor: alternative role in G protein-coupled receptor signaling. Mol Pharmacol 66:880–889
28. Raimondi F, Seeber M, Benedetti PG, Fanelli F (2008) Mechanisms of inter- and intramolecular communication in GPCRs and G proteins. J Am Chem Soc 130:4310–4325
29. Ballesteros J, Weinstein H (1995) Integrated methods for the construction of three-dimensional models and computational

probing of structure-function relations in G protein-coupled receptors. Methods Neurosci 25:366–428
30. Rovati GE (1998) Ligand-binding studies: old beliefs and new strategies. Trends Pharmacol Sci 19:365–369
31. Sali A, Blundell TL (1993) Comparative protein modelling by satisfaction of spatial restraints. J Mol Biol 234:779–815
32. Chen R, Li L, Weng Z (2003) ZDOCK: an initial-stage protein-docking algorithm. Proteins 52:80–87
33. Wall MA, Coleman DE, Lee E, Iniguez-Lluhi JA, Posner BA, Gilman AG, Sprang SR (1995) The structure of the G protein heterotrimer Gi alpha 1 beta 1 gamma 2. Cell 83:1047–1058
34. Im W, Feig M, Brooks CL 3rd (2003) An implicit membrane generalized born theory for the study of structure, stability, and interactions of membrane proteins. Biophys J 85:2900–2918
35. Munson PJ, Rodbard D (1980) LIGAND: a versatile computerized approach for characterization of ligand-binding systems. Anal Biochem 107:220–239
36. De Lean A, Munson PJ, Rodbard D (1978) Simultaneous analysis of families of sigmoidal curves: application to bioassay, radioligand assay, and physiological dose-response curves. Am J Physiol 235:E97–E102
37. Rovati GE, Nicosia S (1994) Lower efficacy: interaction with an inhibitory receptor or partial agonism? Trends Phramcol Sci 15:140–144
38. Draper NR, Smith H (1966) Applied regression analysis. Wiley, New York
39. Walsh M, Foley JF, Kinsella BT (2000) Investigation of the role of the carboxyl-terminal tails of the alpha and beta isoforms of the human thromboxane A(2) receptor (TP) in mediating receptor: effector coupling. Biochim Biophys Acta 1496:164–182
40. Cotecchia S, Exum S, Caron MG, Lefkowitz RJ (1990) Regions of the alpha 1-adrenergic receptor involved in coupling to phosphatidylinositol hydrolysis and enhanced sensitivity of biological function. Proc Natl Acad Sci USA 87:2896–2900
41. Mhaouty-Kodja S, Barak LS, Scheer A, Abuin L, Diviani D, Caron MG, Cotecchia S (1999) Constitutively active alpha-1b adrenergic receptor mutants display different phosphorylation and internalization features. Mol Pharmacol 55:339–347
42. Costa T, Herz A (1989) Antagonists with negative intrinsic activity at delta opioid receptors coupled to GTP-binding proteins. Proc Natl Acad Sci USA 86:7321–7325
43. Costa T, Ogino Y, Munson PJ, Onaran HO, Rodbard D (1992) Drug efficacy at guanine nucleotide-binding regulatory protein-linked receptors: thermodynamic interpretation of negative antagonism and of receptor activity in the absence of ligand. Mol Pharmacol 41:549–560
44. Samama P, Cotecchia S, Costa T, Lefkowitz RJ (1993) A mutation-induced activated state of the beta 2-adrenergic receptor. Extending the ternary complex model. J Biol Chem 268:4625–4636
45. Milligan G (2003) Constitutive activity and inverse agonists of G protein-coupled receptors: a current perspective. Mol Pharmacol 64:1271–1276
46. Kenakin T (2004) Principles: receptor theory in pharmacology. Trends Pharmacol Sci 25:186–192
47. Costa T, Cotecchia S (2005) Historical review: negative efficacy and the constitutive activity of G-protein-coupled receptors. Trends Pharmacol Sci 26:618–624
48. Kenakin T (1997) Agonist-specific receptor conformations. Trends Pharmacol Sci 18:416–417
49. Kobilka BK, Deupi X (2007) Conformational complexity of G-protein-coupled receptors. Trends Pharmacol Sci 28:397–406
50. Park PS, Lodowski DT, Palczewski K (2008) Activation of G protein-coupled receptors: beyond two-state models and tertiary conformational changes. Annu Rev Pharmacol Toxicol 48:107–141
51. Chung DA, Wade SM, Fowler CB, Woods DD, Abada PB, Mosberg HI, Neubig RR (2002) Mutagenesis and peptide analysis of the DRY motif in the alpha2A adrenergic receptor: evidence for alternate mechanisms in G protein-coupled receptors. Biochem Biophys Res Commun 293:1233–1241
52. Lefkowitz RJ, Cotecchia S, Samama P, Costa T (1993) Constitutive activity of receptors coupled to guanine nucleotide regulatory proteins. Trends Pharmacol Sci 14:303–307